Chapter 53
Medical Images Fusion Using Parameterized Logarithmic Image Processing Model and Wavelet Sub-band Selection Schemes

Bole Chang, Wenbing Fan and Bo Deng

Abstract A novel wavelet sub-band selection scheme for medical image fusion, based on the Parameterized Logarithmic Image Processing (PLIP) model, is presented in this chapter which takes the characteristics of human visual system (HVS) and the spatial distribution of wavelet coefficients into account. The different fusion schemes are applied for the different frequency sub-bands. The visibility weighted average method is selected for coefficients in low-frequency band and a variance based weighted method is selected for coefficients in high-frequency bands. Subsequently, the fused coefficients are processed with consistency verification to guarantee the homogeneity of the fused image. Computer simulations illustrate that the proposed image fusion algorithms with the PLIP model is superior to some existing fusion methods, and can get satisfactory fusion results.

Keywords Image fusion · PLIP model · Wavelet transform · Sub-band selection scheme

53.1 Introduction

In the recent years, the study of medical image fusion attracts much attention including diagnosis, research, and treatment. Image fusion is the combination of multimodality source images [1]. Multimodality medical images mainly include the following images, computed tomography (CT) and magnetic resonance imaging (MRI) images and so on [2]. The aim of image fusion is to integrate complementary as well as redundant information from multiple images to create a fused image output, which should contain a more accurate description of the scene and is more suitable for human visual and further image processing and analysis task.

B. Chang (✉) · W. Fan · B. Deng
Department of Information Engineering,
Zhengzhou University, Zhengzhou, China
e-mail: cbl2388@gmail.com

The existing fusion methods involve mainly Pixel Weighted Average fusion (PWA), Laplacian Pyramid (LP), Discrete Wavelet Transform (DWT) [3], Principal Component Analysis (PCA) [4], Contourlet transform (CT) [5], and Nonsubsampled Contourlet Transform (NSCT) [6]. Research shows that the PWA blurs feature information of image. The LP transform decompose fails to introduce any spatial orientation selectivity in the decomposition process. The PCA do not incorporate aspects of the human visual system in their formulation such as sensitivity to edges at their various scales and undesirable side contrast. The Contourlet transform, based on the Laplacian Pyramid and directional filter, is a kind of multi-scale and multi-direction discrete image transformation, in which the process of multi-scale analysis and direction analysis is successively disposed. But it is a varying shift transformation and ignores the relationship between contourlet coefficients. In order to obtain translation invariance, Cunha AL proposed NSCT, which consists of Nonsubsampled Directional Filter Bank (NSDFB) and Nonsubsampled Pyramid (NSP).The NSCT can extract the edge of the image contour information well. But, it captures image detail weakly, and fails to present the local characteristics of image. The DWT of image signal produces non-redundant image representations and provides better spatial and spectral localization of image information. In the DWT scheme, wavelet coefficient fusion rules directly influence the speed and quality of fusion [7].

The chapter is organized as follows: In Sect. 53.2, the PLIP model and the parameterized logarithmic multi-resolution image decomposition structure are described. And a new image fusion algorithm is proposed in Sect. 53.3. Experimental results and analysis are presented in Sect. 53.4. Finally, the conclusions are given with a short summary in Sect. 53.5.

53.2 Wavelet Decomposition Based on PLIP Model

The original concept and theory of wavelet-based multi-resolution analysis came from Mallat [8]. The wavelet transform is a mathematical tool that can detect local time–frequency features in a signal process.

53.2.1 PLIP Model

The PLIP model was proposed by Karen Panetta, which are appropriate particularly for image enhancement in both the spatial and transform domains. With defining a set of parameterized nonlinear operation to replace image of linear operators, it operates image gray value directly. The arithmetical operations of PLIP model are as follows [9].

$$\text{Gray tone calculation: } g(i,j) = M - f(i,j) \tag{53.1}$$

$$\text{Isomorphic transform: } \varphi(g) = -\lambda(M) \cdot \ln^\beta(1 - g/\lambda(M)) \tag{53.2}$$

$$\text{Inverse isomorphic transform: } \varphi^{-1}(g) = \lambda(M)[1 - \exp(-g/\lambda(M))^{1/\beta}] \tag{53.3}$$

where $g(i,j)$ is the same gray tone function and M is the maximum intensity value of input image $f(i,j)$. The parameter $\lambda(M)$ is a linear function of the type $\lambda(M) = AM + B$, with constant parameters A and B. The research shows that visually pleasing images can be got with $\beta = 1$ and $\lambda(M) = 896$.

53.2.2 Image Fusion Based on PLIP Model

The 2D Wavelet decomposition provides a framework in which two dimensional signals are decomposed different level sub-bands, which uses a quadrate mirror set analysis filters, h and g, and synthesis filters, $\tilde{h}$ and $\tilde{g}$ [7]. And the DWT based on the PLIP model (PLIP-DWT) is calculated by making use of the parameterized isomorphic transformation and is defined by the following equations.

$$\text{PLIP - DWT: } W_{\text{PLIP–DWT}}(f) = W_{\text{DWT}}(\varphi(f)) \tag{53.4}$$

$$\text{PLIP - IDWT: } W_{\text{PLIP–IDWT}} = \varphi^{-1}(W_{\text{IDWT}}(W_{\text{PLIP–DWT}}(f))) \tag{53.5}$$

The structures of 2D wavelet decomposition based on the PLIP model analysis and synthesis are shown in Fig. 53.1. The DWT decomposition based on the PLIP
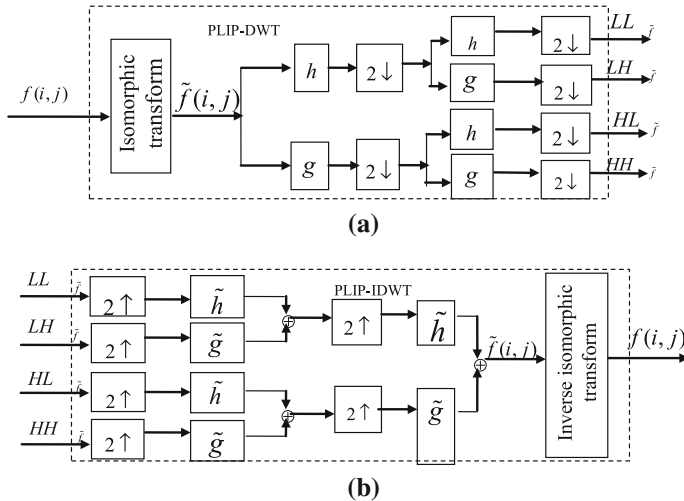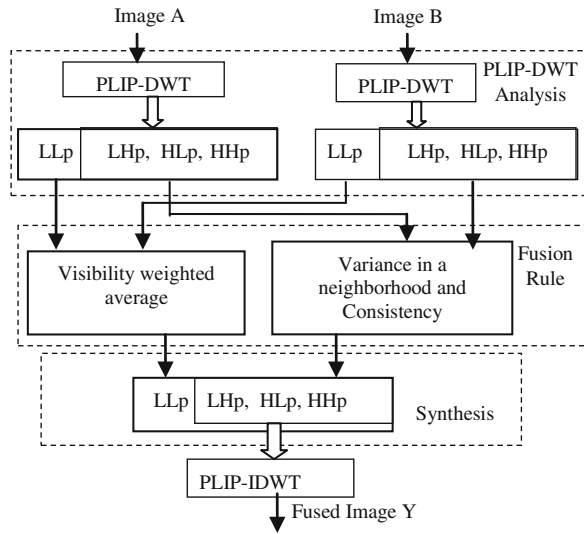

Fig. 53.1 The structures of PLIP 2D wavelet decomposition analysis and synthesis. **a** One stage of 2D PLIP-DWT multi-resolution image decomposition. **b** One stage of 2D PLIP-IDWT multi-resolution image fusion

Fig. 53.2 Schematic diagram of the proposed fusion rule

model generates the low-frequency band coefficient $LL\tilde{f}$ and the high-frequency coefficient $HL\tilde{f}$, $LH\tilde{f}$, and $HH\tilde{f}$.

The overall flowchart of the DWT scheme based on the PLIP model can be illustrated in Fig. 53.2.

53.3 The Proposed Fusion Schemes for the Coefficients

The core technology based on the wavelet transform of the image fusion is the wavelet coefficient fusion rules. Therefore, a new type of wavelet coefficient fusion rules is proposed.

53.3.1 Weighted Average Method in Low Frequency Sub-band

For the low-frequency band, a fusion scheme selects the weighted average method, which is based on HVS to the sensitive degree of image [10]. Two original images, A and B, and their fused image Y are introduced. And the multi-scale decompositions of the original and fused images are denoted by C_A, C_B, and C_Y. Let $p = (m, n, k, l)$ indicates the index corresponding to a particular coefficient. $C_A(p)$ denotes the decomposition value of the corresponding coefficient at the

position (m, n) with decomposition level k and frequency band l (1 = LL, LH, HL, and HH). The visibility of wavelet coefficients is defined as:

$$\omega(p) = \frac{1}{N^2} \sum_{(i,j) \in W_N} \Upsilon(\mu(p)) \cdot (|C(m + i, n + j, k, l) - \mu(p)| / \mu(p)) \quad (53.6)$$

$$\Upsilon(\mu(p)) = (1/\mu(p))^{\alpha} \quad (53.7)$$

$$\mu(p) = (1/N^2) \sum_{(i,j) \in W_N} C(m + i, n + j, k, l) \quad (53.8)$$

where W_N is a $N * N$ block, $\Upsilon(\mu(p))$ is the weighting factor, α is a constant by perceptual experiment, and its range is from 0.6 to 0.7 [10]. After calculating the visibility of all the coefficients in the low-frequency band, the corresponding coefficients with higher magnitude of visibility are then chosen into the fused image as follows:

$$C_Y(p) = (\omega_A(p) \cdot C_A(p) + \omega_B(p) \cdot C_B(p)) / (\omega_A(p) + \omega_B(p)) \quad (53.9)$$

53.3.2 Fusion Scheme in High Frequency Sub-bands

A scheme is proposed by computing the variance in a neighborhood to select the high-frequency coefficients [10]. The neighborhood variance of wavelet coefficient of input image is $\sigma_A(p)$, and the covariance is $\sigma_{AB}(p)$. The $\mu_A(p)$ denotes mean value. The procedure can be formulated as follow.

$$\sigma_A(p) = (1/N^2) \sum_{(i,j) \in W_N} (C_A(m + i, n + j, k, l) - \mu_A(p))^2 \quad (53.10)$$

$$\mu_A(p) = (1/N^2) \sum_{(i,j) \in W_N} C_A(m + i, n + j, k, l) \quad (53.11)$$

$$\sigma_{AB}(p) = (1/N^2) \sum_{(i,j) \in W_N} (C_A(m + i, n + j, k, l) \cdot C_B(m + i, n + j, k, l) - \mu_{AB}(p))^2$$

$$(53.12)$$

$$\mu_{AB}(p) = (1/N^2) \sum_{(i,j) \in W_N} C_A(m + i, n + j, k, l) \cdot C_B(m + i, n + j, k, l) \quad (53.13)$$

The local matching coefficient measure of each sub-band between source images is given as:

$$M_{AB}(p) = 2\sigma_{AB}(p) / (\sigma_A^2(p) + \sigma_B^2(p)) \quad (53.14)$$

Comparing the matching measure to a threshold T determines if detail coefficients are to be combined by simple selection or by weighted averaging.

$$\delta(p) = \begin{cases} 1 - (M_{AB}(p) - T)/2(1 - T), & M_{AB}(p) > T, \sigma_A(p) > \sigma_B(p) \\ (M_{AB}(p) - T)/2(1 - T), & M_{AB}(p) > T, \sigma_A(p) < \sigma_B(p) \\ 1 & M_{AB}(p) < T, \sigma_A(p) > \sigma_B(p) \\ 0 & M_{AB}(p) < T, \sigma_A(p) < \sigma_B(p) \end{cases}$$

$$(53.15)$$

where $\delta(p)$ indicts the factor of multiplicative weight averaging. The fused coefficients are calculated using the following formulation.

$$C_Y(p) = \delta(p) \cdot C_A(p) + (1 - \delta(p)) \cdot C_B(p) \qquad (53.16)$$

53.3.3 Consistency Verification

The proposed method cannot guarantee the homogeneity in the resultant fused image, especially for the high frequency sub-bands [10]. Therefore, a consistency verification scheme can ensure that the dominant features are incorporated into the fused image. The idea is likely to be a 3- by-3 median filter. And a window-based verification is applied to the fused high frequency coefficients. In the implementation, this rule is applied to a binary decision map, followed by the application of a median filter. This process can be formulated as follows:

$$C_A^m(p) = \underset{(i,j) \in W_N}{\text{median}}(|C_A(m + i, n + j, k, l)|) \qquad (53.17)$$

$$\beta(p) = \begin{cases} 1, & C_A^m(p) > C_B^m(p) \\ 0, & \text{otherwise} \end{cases} \qquad (53.18)$$

$$\beta'(p) = \sum_{(i,j) \in W_N} \beta(m + i, n + j, k, l) \qquad (53.19)$$

$$\beta^*(p) = \begin{cases} 1, & \beta'(p) > N \\ 0, & \text{otherwise} \end{cases} \qquad (53.20)$$

Refer to (53.16), the fused coefficients in the high frequency sub-bands are modified by:

$$C_Y^*(p) = C_Y(p) + \lambda \cdot [\beta^*(p) \cdot C_A(p) + (1 - \beta^*(p)) \cdot C_B(p)] \qquad (53.22)$$

where λ is a constant by perceptual experiment?

53.4 Experimental Results and Analysis

In this section, the performance of the proposed method is compared with those of PWA, LP, PCA, Contourlet transform, NSCT and DWT. The first experiment is tested on MRI and MRA images, as shown in Fig. 53.3. And the information entropy (IE), cross entropy (CE), mutual information (MI) and fusion symmetry (FS) of the fused image are applied to evaluate the performance of the above fusion method [11]. The performances of the different methods are listed in Table 53.1.

Comparing the experimental results, the proposed method of fusion visibility is the best. As is shown from Table 53.1, the IE of the proposed method is higher than results of other methods, and the values of CE and FS are lower than the results of other methods. And the proposed fusion scheme removes the blurring information and the fused image has more resolution than other methods.
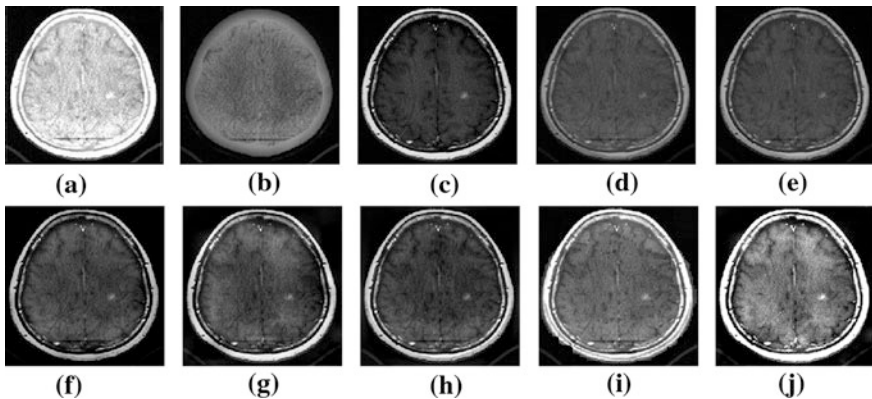

Fig. 53.3 Fusion results of the MRI and MRA images with different methods. **a** Reference image; **b** Original MRI image; **c** Original MRA image; **d** Fused image by PWA method; **e** Fused image by PCA method; **f** Fused image by LP method; **g** Fused image by DWT method; **h** Fused image by Contourlet transform method; **i** Fused image by NSCT method; **j** Fused image by the proposed method

Table 53.1 Quantitative evaluation results of different fusion methods in Fig. 53.3

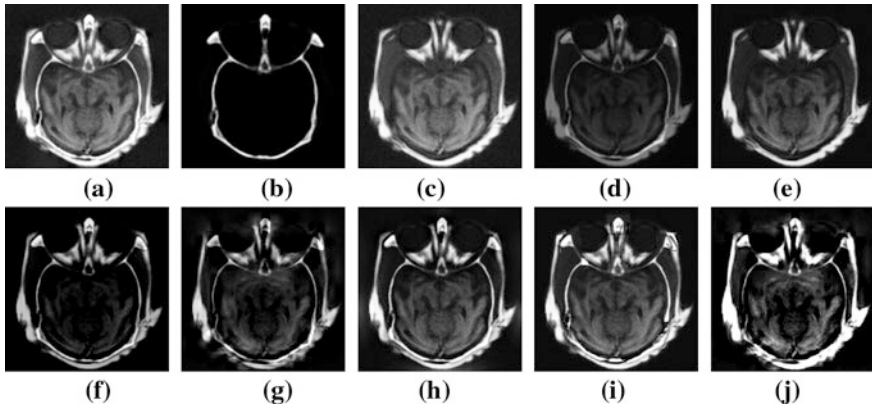| Fusion methods	IE	CE	MI	FS
PWA	6.3195	1.4806	3.2325	0.0054
PCA	6.4163	1.3954	2.9406	0.0199
LP	5.8181	1.3732	2.2674	0.1035
DWT	6.0208	1.5649	2.6369	0.1623
Contourlet transform	6.4335	1.6156	2.7337	0.1845
NSCT	6.4862	1.3823	2.9891	0.0183
Proposed method	6.4919	1.3305	2.4366	0.0013

Fig. 53.4 Fusion results of the "brain" CT and MRI images with different methods. **a** Reference image; **b** Original CT image; **c** Original MRI image; **d** Fused image by PWA method; **e** Fused image by PCA method; **f** Fused image by LP method; **g** Fused image by DWT method; **h** Fused image by Contourlet transform method; **i** Fused image by NSCT method; **j** Fused image by the proposed method

Table 53.2 Quantitative evaluation results of different fusion methods in Fig. 53.4

Fusion methods	IE	CE	MI	FS
PWA	5.9152	0.7407	2.5326	0.1015
PCA	6.5814	0.4396	2.2358	0.0797
LP	3.8037	1.3318	2.0654	0.7059
DWT	5.9748	0.6800	1.6721	0.4652
Contourlet transform	6.9694	0.1332	1.9381	0.0733
NSCT	6.7896	0.1939	2.4606	0.0984
Proposed method	5.7291	0.1206	2.6832	0.0636

For further comparing, the proposed method is tested on CT and MRI images as shown in Fig. 53.4. The relevant performances of the different methods are listed in Table 53.2.

Comparing the experimental results in Fig. 53.4, the proposed method of fusion visibility is the best. As is shown from Table 53.2, the MI of the proposed method is higher than results of other methods, and the values of CE and FS are lower than the results of other methods. And the proposed fusion scheme contains more image information and the fused image has more resolution than other methods.

53.5 Conclusion

A novel wavelet-based sub-band selection approach with PLIP model is presented for medical image fusion—it consists of four steps: isomorphic transform, wavelet decomposition, coefficients fusion, wavelet synthesis, and inverse isomorphic

transform. The experimental results show that the proposed fusion method outperforms some existing fusion methods and it can get satisfactory fusion results.

References

1. Piella, G.: A general framework for multi-resolution image fusion: From pixels to regions. Inf. Fusion **4**, 259–280 (2003)
2. Yang, Y., Park, D.S., Huang, S., Rao, N.: Fusion of CT and MR images using an improved wavelet based method. J. X-Ray Sci. Technol. **18**(10), 157–170 (2010)
3. Wang, Y., Lohmann, B.: Multi-sensor image fusion: Concept, method and applications. Technical Report, Institute of Automatic Technology, University of Bremen, Bremen, Germany (2000)
4. Pradhan, P.S., et al.: Estimation of the number of decomposition levels for a wavelet-based multi-resolution multi-sensor image fusion. IEEE Trans. Geosci. Remote Sens. **44**(12), 3674–3686 (2006)
5. Do, M.N., Vetterli, M.: The contourlet transform: An efficient directional multi-resolution image representation. IEEE Trans. Image Process. **14**(12), 2091–2106 (2005)
6. Cunha, A.L., Zhou, J.P., Do, M.N.: The nonsubsampled contourlet transform: Theory, design, and applications. IEEE Trans. Image Process. **15**(10), 3089–3101 (2006)
7. Cheng, S.L., He, J.M., Lv, Z.W.: Medical image of PET/CT weighted fusion based on wavelet transform. In: iCBBE'08, pp. 2523–2525 (2008)
8. Mallat, S.G.: A theory for multi-resolution signal decomposition: The wavelet representation. IEEE Trans. Pattern Anal. Mach. Intell. **11**(7), 674–693 (1989)
9. Nercessian, S.C., Panetta, K.A., et al.: Multi-resolution decomposition schemes using the PLIP with application to image fusion. EURASIP J. Adv. Signal Process. **2011**(515084), 17p (2011)
10. Huang, J.W., Yun, Q.S., Dai, X.H.: A segmentation-based image coding algorithm using the features of human vision system. J. Image Graph. **4**(5), 400–404 (1999)
11. Shi, W.Z., et al.: Wavelet based image fusion and quality assessment. Int. J. Appl. Earth Obs. Geoinf. **6**(3–4), 241–251 (2005)